In Vivo and in Vitro activity of colistin-conjugated bimetallic silver-copper oxide nanoparticles against Pandrug-resistant *Pseudomonas aeruginosa*

Asmaa Abdul Hak[1], Hamdallah H. Zedan[2], Hadir A. El-Mahallawy[3], Gharieb S. El-Sayyad[1,4,5]* and Mai M. Zafer[1]*

Abstract

Background Addressing microbial resistance urgently calls for alternative treatment options. This study investigates the impact of a bimetallic formulation containing colistin, silver, and copper oxide on a pandrug-resistant, highly virulent *Pseudomonas aeruginosa (P. aeruginosa)* isolate from a cancer patient at the National Cancer Institute, Cairo University, Egypt.

Methods Silver nanoparticles (Ag NPs), copper oxide nanoparticles (CuO NPs), and bimetallic silver-copper oxide nanoparticles (Ag-CuO NPs) were synthesized using gamma rays, combined with colistin (Col), and characterized by various analytical methods. The antimicrobial activity of Col-Ag NPs, Col-CuO NPs, and bimetallic Col-Ag-CuO NPs against *P. aeruginosa* was evaluated using the agar well diffusion method, and their minimum inhibitory concentration (MIC) was determined using broth microdilution. Virulence factors such as pyocyanin production, swarming motility, and biofilm formation were assessed before and after treatment with bimetallic Col-Ag-CuO NPs. The in vivo efficacy was evaluated using the *Galleria mellonella* model, and antibacterial mechanism were examined through membrane leakage assay.

Results The optimal synthesis of Ag NPs occurred at a gamma ray dose of 15.0 kGy, with the highest optical density (OD) of 2.4 at 375 nm. Similarly, CuO NPs had an optimal dose of 15.0 kGy, with an OD of 1.5 at 330 nm. Bimetallic Ag-CuO NPs were most potent at 15.0 kGy, yielding an OD of 1.9 at 425 nm. The MIC of colistin was significantly reduced when combined with nanoparticles: 8 µg/mL for colistin alone, 0.046 µg/mL for Col-Ag NPs, and 0.0117 µg/mL for Col-Ag-CuO NPs. Bimetallic Col-Ag-CuO NPs reduced the MIC four-fold compared to Col-Ag NPs. Increasing the sub-inhibitory concentration of bimetallic nanoparticles from 0.29×10^{-2} to 0.58×10^{-2} µg/mL reduced *P. aeruginosa* swarming by 32–64% and twitching motility by 34–97%. At these concentrations, pyocyanin production decreased by 39–58%, and biofilm formation was inhibited by 33–48%. The nanoparticles were non-toxic to *Galleria mellonella*, showing 100% survival by day 3, similar to the saline-treated group.

*Correspondence:
Gharieb S. El-Sayyad
Gharieb.Elsayyad@acu.edu.eg; Gharieb.Elsayyad@gu.edu.eg
Mai M. Zafer
maizafer@acu.edu.eg
Full list of author information is available at the end of the article

Conclusions The synthesis of bimetallic Ag-CuO NPs conjugated with colistin presents a promising alternative treatment for combating the challenging *P. aeruginosa* pathogen in hospital settings. Further research is needed to explore and elucidate the mechanisms underlying the inhibitory effects of colistin-bimetallic Ag-CuO NPs on microbial persistence and dissemination.

Keywords Bimetallic nanoparticles, Antimicrobial activity, *Pseudomonas aeruginosa*, Antimicrobial resistance, Virulence factors

Introduction

Pseudomonas aeruginosa poses a crucial threat as an opportunistic pathogen in hospital environments [1]. Recognizing its exceptional resistance profile, the World Health Organization categorized it as critically prioritized for the development of new antibiotics [2].

The adaptability of *P. aeruginosa* genome, coupled with its biofilm-forming proficiency and array of virulence factors, underscores its pathogenicity, particularly in immunocompromised cancer patients, leading to elevated mortality rates [3]. Antimicrobial resistance, a global challenge, complicates treatment options, particularly in countries like Egypt [4, 5].

Reports of *P. aeruginosa* strains resistant even to colistin have surfaced, amplifying public health concerns [6, 7]. This phenomenon is exacerbated by the overuse and misuse of antibiotics, coupled with socioeconomic factors such as inadequate hygiene practices and lax infection control measures [8–10]. Infections caused by pandrug-resistant *P. aeruginosa* not only heighten mortality rates but also disrupt anticancer therapies [11]. Therefore, there is an urgent need for innovative antimicrobial agents effective against this resilient pathogen. Nanoparticles (NPs) have emerged as a promising strategy to combat multidrug-resistant bacterial infections [12, 13]. Metal-based nanoparticles, in particular, exhibit antibacterial properties, primarily through mechanisms involving reactive oxygen species and bacterial membrane disruption [14, 15]. Combining antibiotics with metal nanoparticles enhances antibacterial efficacy, with the increased surface area of nanoparticles facilitating bacterial cell damage [16].

The unique properties of bimetallic nanomaterials, stemming from synergistic effects between different metallic components, have gained significant interest [17–19]. Notably, bimetallic silver-copper oxide nanoparticles (Ag-CuO NPs) have demonstrated versatile plasmonic properties, making them attractive for various applications, including sensors and catalysis [20].

In this study, we investigated the antibacterial and anti-virulence potential of the synthesized mono- and bimetallic formulations of colistin-conjugated silver and copper oxide nanoparticles against pandrug-resistant and highly virulent clinical isolate of *P. aeruginosa*, obtained from immunocompromised hospitalized pediatric cancer patient.

Materials and methods

Chemicals and reagents

The production of NPs was applied using analytical-grade chemicals such as Ag NO_3 and $CuSO_4 \cdot 5H_2O$ (Sigma Aldrich, UK). Muller-Hinton agar and broth, Tryptic Soy Broth (TSB) used for microbiological testing were obtained from Oxoid, UK.

Gamma radiation

Processes for gamma irradiation were carried out at the National Center for Radiation Research and Technology (NCRRT) in Cairo, Egypt. The samples were gamma-irradiated in solution form using ^{60}Co-Gamma chamber 4000-A-India as the radiation source, with the radiation time being calculated to be 0.843 kGy per hour (dose rate).

Synthesis of Col-Ag NPs, Col-CuO NPs and bimetallic Col-Ag-CuO NPs

Ag NPs, CuO NPs, and bimetallic Ag-CuO NPs were synthesized using gamma rays (as a both direct and indirect reducing tool). Because powerful reducing electrons, known as e$^-_{aq}$, were freed by gamma rays in aqueous solutions, metal ions were subsequently reduced. This process is known as direct reduction. While the radiolysis byproducts H$^•$ and OH$^•$ interact, and reduce metal ions, the indirect reduction was caused by H$^•$ and OH$^•$ [13].

Several solution samples (50 mL) containing (1.0 mM) Ag NO_3 were combined with colistin sulphate solution to create Ag NPs. Similarly, numerous solution (50 mL) of (1.0 mM) $CuSO_4 \cdot 5H_2O$ were combined with colistin sulphate solution to synthesize CuO NPs. Multiple solution samples containing (1.0 mM; 25 mL) Ag NO_3 and (1.0 mM; 25 mL) $CuSO_4 \cdot 5H_2O$ were combined with colistin sulphate solution to synthesize bimetallic Ag-CuO NPs.

Prior to gamma radiation, the pH of each sample was determined and adjusted to neutral (pH 7). Then, fixed dosages of gamma radiation (15 kGy) were applied to the solutions at room temperature. The optical density (OD.) of the generated NPs at a particular and defined wavelength was measured using UV-Vis. spectra. In the case of bimetallic Ag-CuO NPs, the relative Ag/CuO concentration was studied as it is a major determinant in addition to the dosage [21, 22].

Abdul Hak *et al. BMC Microbiology*   (2024) 24:213

Page 3 of 17

Characterization of the synthesized NPs

Using a UV-Vis. spectrophotometer (JASCO V-560) at certain wavelengths, the absorbance and optical properties of produced Col-Ag NPs, Col-CuO NPs, and bimetallic Col-Ag-CuO NPs were examined. For Auto-zero reasons, a sample devoid of any metal ions was additionally included. All samples were initially screened for optical characteristics and to establish the fixed wavelengths used to calculate absorbance. To ascertain the mean size distribution of the produced NPs, measurements of dynamic light scattering were made at the St. Barbara, California, USA facility using the DLS-PSS-NICOMP 380-ZLS particles sized system. 100 μL of NPs specimens were transferred to a temporary, tiny cuvette. Five procedures were carried out after equilibration at a temperature of 25 ± 2 °C for 2.0 min. In addition, the form, appearance, and average particle size of the produced NPs were investigated using a high-resolution transmission electron microscope (HR-TEM, JEM2100, Jeol, Japan). NPs samples used for TEM studies were drop-coated into carbon-coated TEM grids following dried in an incubator at 37.0 ± 2 °C. Additionally, using the XRD-6000 lists, Shimadzu equipment, SSI, Japan, it was possible to assess the crystallization, crystallite size, and/or structure of the generated NPs. The magnitude of the diffracted X-rays was measured using the diffracted angle 2θ. To clarify surface shape, border size, and the distribution of the generated NPs surrounding GA, an analysis using SEM (SEM, ZEISS, EVO-MA10, Germany) was performed.

Bacterial strain

The study was conducted using a clinical isolate of *P. aeruginosa* obtained from the blood culture of a pediatric cancer patient hospitalized at the National Cancer Institute, Cairo University, Egypt, in September 2022. The *P. aeruginosa* isolate was initially identified using standard microbiological techniques such as gram staining and oxidase testing. Further confirmation was conducted using the Vitek® 2 automated system (bioMérieux, Marcyl'Etoile, France) in the microbiology laboratory at the National Cancer Institute. This isolate was selected from a collection of isolates for its high virulence and susceptibility profile. It exhibited strong biofilm production, pyocyanin production, and demonstrated lethality in the *Galleria mellonella* model.

Antimicrobial susceptibility testing

Antimicrobial susceptibility testing was conducted using VITEK 2 automated machine (bioMérieux, Marcy l'Etoile, France) against a panel of antibiotics including ceftazidime, cefazolin, cefuroxime, ceftriaxone, cefepime, ampicillin, amoxicillin-clavulanate, piperacillin-tazobactam, ceftolozane-tazobactam, amikacin, gentamicin, ertapenem, imipenem, meropenem, trimethoprim-sulfamethoxazole, nitrofurantoin, ciprofloxacin, levofloxacin, and tigecycline. Interpretation of results was based on CLSI guidelines [23]. Colistin susceptibility was assessed using the broth microdilution method and interpreted according to EUCAST guidelines [24].

In-vitro Antimicrobial activity of Col-AgNPs and Col-Ag-CuONPs

The antimicrobial activity of Col-Ag NPs, Col-CuO NPs, and Col-Ag-CuO NPs composites was assessed using the agar well diffusion method [25]. A suspension of *P. aeruginosa* isolate at a concentration of 1×10^8 CFU/mL was prepared and streaked on Muller-Hinton agar plates (Oxoid, UK). Three concentrations (100%, 50%, and 25%) of Col-Ag NPs, Col-CuO NPs, and Col-Ag-CuO NPs were tested, with 50 μL of each concentration added to the wells. Incubation of the plates at 37 °C for 24 h allowed evaluation of antimicrobial activity by measuring the diameters of the zones of inhibition. The experiments were conducted in triplicate, and average results were calculated.

For the determination of minimum inhibitory concentration, the least effective concentration of Col-Ag NPs, Col-CuO NPs, and Col-Ag-CuO NPs observed in the agar well diffusion assay was utilized to generate a wide range of serial dilutions in a 96-well plate using cation-adjusted Muller–Hinton (CAMH) broth. The concentration of colistin within this range was 25 μg/mL, with concentrations spanning from 25 to 3×10^{-6} μg/mL in the 96-well plate. A cell suspension was prepared by suspending 3 colonies of overnight growth in saline to achieve a density of 1×10^8 CFU/mL. This suspension was further diluted to 5×10^6 CFU/mL using cation-adjusted Muller–Hinton (CAMH) broth. Subsequently, 10 μL of the inoculum was transferred to the wells containing 100 μL of the diluted preparations to attain a final inoculum size of 5×10^5 CFU/mL. The plates were then incubated at 37 °C for 24 h [26].

Anti-virulence activity

Motility test

The impact of the bimetallic Col-Ag-CuO NPs alloy on *P. aeruginosa* swarming and twitching motilities was investigated following the method outlined by Luo et al. [25]. An overnight culture of *P. aeruginosa* grown in Luria Bertani broth (LB) was adjusted to reach an $OD_{600} = 1$. The swarming medium was prepared by supplementing LB with 0.5% (w/v) casamino acids and 0.4% (w/v) Bacto agar, while the twitching medium consisted of 1.5% LB agar. Two sub-inhibitory concentrations of the Col-Ag-CuO NPs alloy were added to the agar media prior to solidification (Concentration $1 = 0.29 \times 10^{-2}$ μg/mL, Concentration $2 = 0.58 \times 10^{-2}$ μg/mL), and then 2.5 μL of

the inoculum was applied to the swarming and twitching agar plates, followed by incubation at 35 °C for 24 h. The migration zones appearing on the agar plates were monitored. All motility experiments were conducted in triplicate.

Pyocyanin production

The pyocyanin production assay was conducted following the protocol outlined by Wang et al. [27]. Briefly, a culture of *P. aeruginosa* isolate was grown in P*seudomonas* broth supplemented with two sub-inhibitory concentrations of Col-Ag-CuO NPs alloy (Concentration $1 = 0.29 \times 10^{-2}$ μg/mL, Concentration $2 = 0.58 \times 10^{-2}$ μg/mL) at 37 °C for 24 h. The culture was then centrifuged, and the supernatant collected. Subsequently, the supernatant was mixed with chloroform by vortexing and centrifuged at 8000 rpm for 10 min. The resulting mixture was then combined with 0.2 M HCl in a new centrifuge tube and centrifuged again. The organic layer was removed, and the absorbance of pyocyanin was measured at 520 nm.

Biofilm formation

Overnight cell growth in Tryptic Soy Broth (TSB) was diluted (1:100) and added to a 96-well microtiter plate, with one set of wells serving as a control and the others treated with two sub-inhibitory concentrations of the nanocomposite solution (Conc. $1 = 0.29 \times 10^{-2}$ μg/mL, Conc. $2 = 0.58 \times 10^{-2}$ μg/mL). The plate was then incubated at 35 °C for 24 h without agitation. Planktonic cells were removed, and the attached cells were washed with phosphate buffer solution (PBS), air dried for 15 min, and stained with 0.1% crystal violet for 30 min at room temperature. After washing off the dye, the stained biofilm was dissolved using 33% glacial acetic acid, and the OD was measured at a wavelength of 570 nm [28].

The same procedure was repeated to evaluate the effect of the nanocomposites on mature pre-formed biofilms of *P. aeruginosa*. In this case, overnight bacterial cultures were allowed to form biofilms in the microtiter plate for 24 h at 35 °C without agitation. After removing planktonic cells, fresh TSB media containing different concentrations of the alloy were added to the wells with attached cells and incubated for an additional 24 h at 35 °C [29]. Biofilm disruption ability was determined by measuring the OD at 570 nm after staining with crystal violet dye. Each test was performed in triplicate, and the average value was calculated. Furthermore, another set of cultures, not stained with crystal violet, underwent viable count analysis. Attached cells were scratched with a micropipette tip and dispersed in saline using dilutions up to 10^{-5} to assess the survival ability of biofilm cells in the presence of the nanocomposite in both scenarios [30].

In vivo activity using *Galleria mellonella model*

The method employed in this study was implemented according to Thomaz et al. [31]. *G. mellonella* larvae weighing between 150 and 220 mg, obtained in the final (7th) larval instar, were selected for experimentation. Only larvae exhibiting robust movement and free of myelinization were utilized. Five groups, each consisting of 10 *G. mellonella* larvae, were monitored for a duration of 72 h. The experimental groups were configured as follows:

1. Positive control: Larvae were injected with 10 μL of overnight culture of the *P. aeruginosa* clinical isolate, adjusted in saline to reach a concentration of 10^4 CFU/mL.
2. Toxicity assessment: Larvae were injected with 10 μL of the higher concentration of the nanocomposite (Conc. $2 = 0.58 \times 10^{-2}$ μg/mL).
3. Treatment groups: Larvae were treated with either concentration 1 (0.29×10^{-2} μg/mL) or concentration 2 (0.58×10^{-2} μg/mL) of the nanocomposite. After a 2-hour incubation at 28 °C, these groups were infected with 10 μL of the bacterial strain, similar to the positive control group.
4. Negative control: Larvae were injected with 10 μL of saline.

Injection was administered into the haemocoel of the last right pro-leg using a 10 μL Hamilton micro syringe. The larvae were then placed in Petri dishes and incubated at 37 °C, with monitoring conducted over the course of 72 h. Survival curves were constructed based on the criteria of live or dead observations.

Effect of the synthesized NPs on protein leakage from *P. aeruginosa* cell membranes

Pure 18 h *P. aeruginosa* culture was set at 0.5 McFarland (1×10^8 CFU/mL) and 100 μL was injected into 10 mL of the nutrient broth containing well-sonicated and dispersed Col-Ag NPs, Col-CuO NPs, and Col-Ag-CuO NPs at various concentrations (0.125, 0.25, 0.5, and 1.0 mg/mL). Nanocomposites-free broth injected with culture had been used as the control. All the treated samples were incubated at 37 °C for 5 h. and then centrifuged for 15 min. at 5000 rpm [32]. For the different samples, 100 μL supernatant was combined with 1 mL of Bradford reagent. Optical density was then measured at 595 nm in the next 10 min of dark incubation [32].

Statistical analysis

ONE WAY ANOVA at P 0.05, the least significant difference (LSD) summary, and Duncan's multiple regions were used to statistically analyze the obtained results

[33]. Using SPSS software (version 15), analyses and evaluations of the data and findings were conducted.

Results and discussion
Synthesis of Col-Ag NPs, Col-CuO NPs and Col-Ag-CuO NPs
Gamma-rays screening of the produced Col-Ag NPs, Col-CuO NPs and Col-Ag-CuO NPs using a UV-Vis. spectrophotometer is shown in Fig. 1. According to Fig. 1, the dosage of 15.0 kGy that produces Ag NPs with the greatest OD. = 2.4 (diluted a total of two times) at 375.0 nm is the most efficient used for their synthesis. In a similar vein, Fig. 1 demonstrates that the optimal dosage for the creation of CuO NPs is 15.0 kGy gamma rays, with an OD. of 1.5 (diluted five times) at 330.0 nm. However, Fig. 1 shows that the most effective dosage for the production of bimetallic Ag-CuO NPs is 15.0 kGy, which has a high OD. of 1.9 (diluted five times) at 425.0 nm. Gamma rays were used in this instance to produce consistent NPs with a high relative yield without the need of high temperatures or a different reducing chemical agents [34, 35].

The proportional productivity of the produced NPs had reduced when the dosage was increased by more than 15 kGy, because excess free radicals and solvated electrons (created by water radiolysis) alter the pH of the solutions, target newly formed NPs (which have different charges), interact with them, and eventually form aggregated NPs, which reduce their level of intensity in the UV-Vis. spectrum, elevated radiation is not helpful in the synthesis of new nanoparticles.

It is astonishingly discovered that the surface Plasmon resonance (SPR) of bimetallic Ag-CuO NPs solutions caused them to display a rich brownish pink hue [36, 37]. The fabrication of bimetallic Ag-CuO NPs at an elevated relative yield with low Ag and high Cu content demonstrates the current data's scientific viability by avoiding the hazardous effects of Ag NPs in the generated bimetallic Ag-CuO NPs. Silver nanoparticles (Ag NPs) were reported in the literature to have high antimicrobial activity. However, at low concentrations, Ag NPs were found to be toxic, but when combined with copper nanoparticles (CuO NPs) to form what is known as bimetallic NPs the toxicity and the dangerous effect will be reduced. In this study, we attempted to lower the toxicity of the prepared Ag NPs by combining them with CuO NPs as one alloy as mentioned in our recent published bimetallic NPs papers [38–48].

Characterization of Col-Ag NPs, Col-CuO NPs and Col-Ag-CuO NPs conjugates
SEM analysis
Figure 2 depicts the appearance, and surface shape of the synthesized Col-Ag NPs, Col-CuO NPs and Col-Ag-CuO NPs. Figure 2a shows that Col-Ag NPs, which appeared as brilliant particles, were evenly spread in identical form. The SEM examination of Col-CuO NPs, which likewise emerged as brilliant particles, is also shown in Fig. 2b. The SEM confirmations of the synthesized bimetallic Col-Ag-CuO NPs are shown in Fig. 2c. According to Fig. 2d, Ag and CuO NPs were dispersed uniformly.
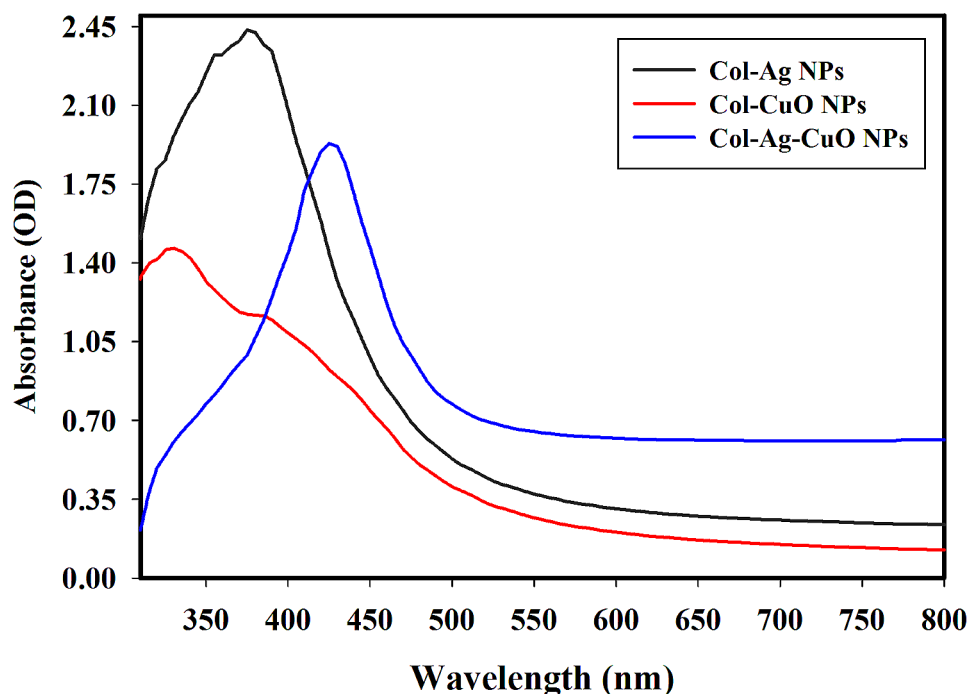

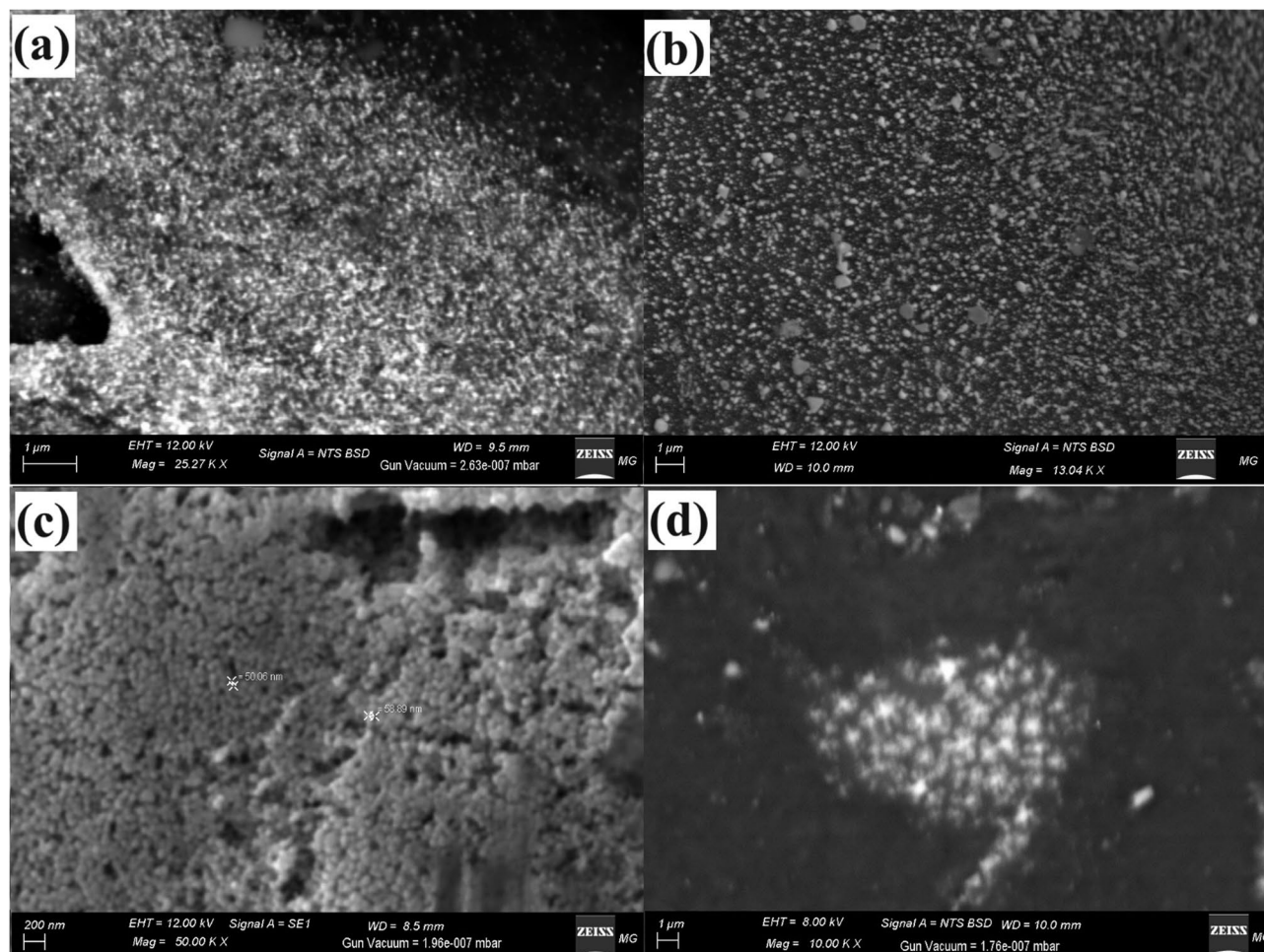**Fig. 1** UV-Vis. spectra for the synthesized Col-Ag NPs, Col-CuO NPs and bimetallic Col-Ag-CuO NPs by 15 kGy gamma rays

Fig. 2 Surface morphology determination for the synthesized Col-Ag NPs **(a)**, Col-CuO NPs **(b)** and bimetallic Col-Ag-CuO NPs **(c**, and **d)** using SEM imaging

The bond formed between the colistin drug, and the synthesized NPs was intermolecular hydrogen bond as the results confirmed by FTIR analysis in recent publication [49].

The produced Ag, Cu, and Ag-CuO bimetallic NPs (in the present study) were uniformly distributed with wide size and the same spherical shape, according to a comparison of the literature about the morphological shape and analysis of elements.

Bimetallic silver and gold core-shell NPs were created by Mohsin et al. [50] using the citrate reduction process at various pH levels and temperatures. The acquired morphological form and boundary size suggested that they had a size varied from 50 to 65 nm and seem as spherical particles, which means that both pH and temperature play a crucial role in the creation process. Finally, our findings were compared with the newly published studies [51–54].

HR-TEM analysis

HR-TEM analysis was used for the characterization of shape and size of the synthesized nanoparticles (Fig. 3). It was possible to determine the mean size of the particles and see how the manufactured Col-Ag NPs, Col-CuO NPs, and bimetallic Col-Ag-CuO NPs appeared. Additionally, data from HR-TEM and DLS measurements were compared. The produced Col-Ag NPs, Col-CuO NPs, and bimetallic Col-Ag-CuO NPs have a variety of forms, including oval and spherical morphologies, as seen in HR-TEM pictures.

Col-Ag NPs varied in size from 48.9 nm to 93.3 nm, with a median diameter of 67.5 nm, as shown in Fig. 3a. Figure 3b shows the diameter range of Col-CuO NPs, which varied from 24.1 nm to 90.9 nm with a mean diameter of 68.89 nm (Fig. 3b). The dimension of bimetallic Ag-CuO NPs, on the other hand, is shown in Fig. 3c and d; it varied from 25.2 nm to 92.2 nm, with a mean diameter of 56.5 nm (Fig. 3d).

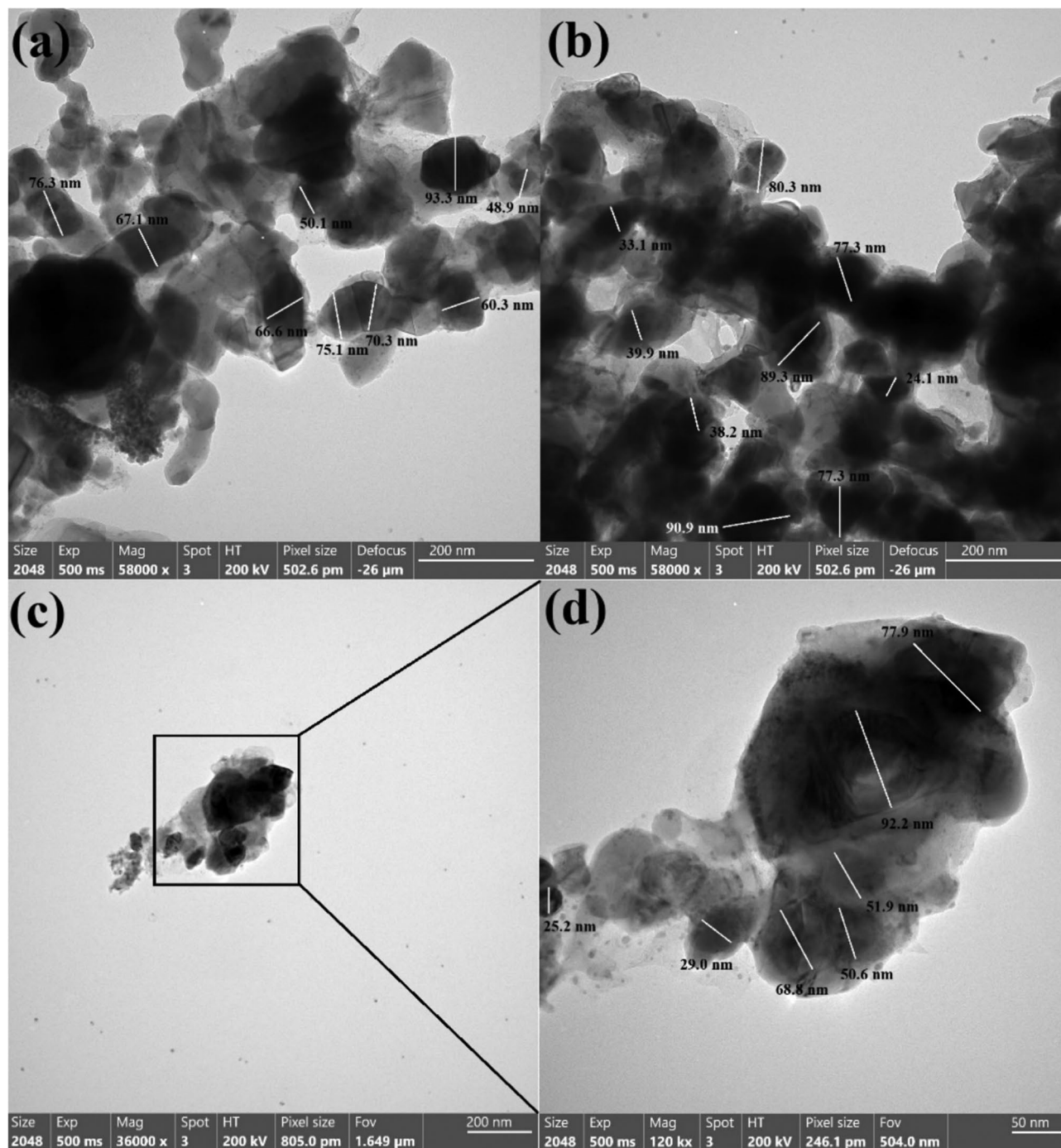The produced Ag, CuO, and bimetallic Ag-CuO NPs varied in size and were mostly spherical in form,

Fig. 3 Shape, and size determination for the synthesized Col-Ag NPs **(a)**, Col-CuO NPs **(b)** and bimetallic Col-Ag-CuO NPs **(c**, and **d)** using HRTEM imaging

according to a comparison of average particle size and shape in the literature. By using the extract of a filamentous fungus, Castro-Longoria et al. [55], synthesized silver, gold, and silver-gold bimetallic. When the fungus was subjected to the water solutions of 10^{-3} M of $AgNO_3$ and $HAuCl_4$, respectively, the shape of the NPs was found to be mainly spherical with a mean diameter of 11.0 nm for silver and 32.0 nm for gold.

Although different morphologies may be noticed owing to the synthetic process from extract, the anisotropic shape had been recorded, the created forms in that work [55], may be varied as the shape of extracted NPs was roughly circular or ellipsoidal in all cases. Due to the use of only one reducing and capping agent, a constant form is seen in our investigation. Finally,

our findings were compared with the newly published studies [56–59].

DLS analysis

In order to assess the distribution of particle sizes and determine the mean size of particles for Ag NPs produced by gamma radiation in the presence of colistin, DLS analysis was carried out to find out particle size distribution. The results are shown in Fig. 4a as 181.34 nm. It was investigated to be 190.25 nm for bimetallic Ag-CuO NPs (Fig. 4c) and 189.25 nm for CuO NPs (Fig. 4b).

It is important to note that the colistin used, which served as a suitable capping and stabilizing agent, was responsible for the creation of the mono-distributed NPs [60]. As DLS analysis measures the hydrodynamic diameter of NPs bound by molecules of water (solvent), resulting in bigger sizes of the capped NPs, and HR-TEM analysis calculates the real particle size of the substance lacking solvent layer, it is common for DLS size measurements to develop greater in values compared to HR-TEM measurements [61]. The NPs that were produced were highly dispersed in a restricted range of sizes due to the scientific validity of DLS, which significantly improved their characteristics and applications [62].

XRD analysis

The XRD studies for the generated NPs are shown in Fig. 5. The amorphous and crystal orientations in the produced NPs, respectively, indicate which is a precursor and the produced Col-Ag NPs, Col-CuO NPs, and Col-Ag-CuO NPs. The XRD diffraction peaks of Col-Ag NPs were displayed in Fig. 5, including peaks at 2Ɵ = 38.22º, 44.18º, 63.49º, and 78.25º that were associated with the typical card JCPDS-ICDD number 04-0783 and resembled (111), (200), (220), and (311) Bragg's reflections [13, 63], The XRD of the synthesized Col-CuO NPs, however, revealed unique peaks at 2Ɵ = 31.23º, 36.81º, 39.89º, 51.56º, 59.86º, 67.12º, and 70.18º that were accompanied by a distinctive card JCPDS number 892,531 and related to Bragg's reflections (110), (002), (200), (202), (020), (022), and (220) [64].

Additionally, Fig. 5 displays the XRD findings of the produced bimetallic Col-Ag-CuO NPs and emphasizes the XRD diffraction peaks of Ag NPs, such as peaks at 2Ɵ = 38.22º, 44.18º, 63.49º, and 78.25º, that are accompanied by a standard card JCPDS number 361,451, and match the (111), (200), (220), and (311) Bragg's reflections [65].

The angles (110), (002), (200), (202), (020), (022), and (220) of Bragg's reflections are represented by the Col-CuO NP diffraction peaks at 2Ɵ = 30.19º, 36.19º, 40.12º, 52.09º, 58.40º, 67.40º, and 71.19º, that are supplemented by the standard card JCPDS number 892,531 [64].

The produced Col-Ag-CuO NPs were crystallized and possessed a face-centered (fcc) crystalline structure,

according to the available XRD data (Fig. 5). According to the XRD data, the produced bimetallic NPs were extremely crystalline and associated with amorphous colistin , which increased their movement in the solution to enhance application [66].

The middle crystallite size of Ag NPs, CuO NPs, and bimetallic Col-Ag-CuO NPs were defined using the equation of Williamson-Hall (WH) [67, 68], and the values supplied to Eq. 1 were discovered to be 38.4 nm, 39.5 nm, and 34.7 nm, respectively.

$$\beta\cos\theta = \frac{k\lambda}{D_{W-H}} + 4\epsilon\sin\theta \tag{1}$$

Antimicrobial susceptibility

The *P. aeruginosa* isolate utilized in this study demonstrated complete resistance (100%) to all tested antimicrobial classes. Moreover, the isolate exhibited non-susceptibility to colistin, with a minimum inhibitory concentration (MIC) of 8 µg/mL. The susceptibility screening results unequivocally indicate that our *P. aeruginosa* isolate is pan-drug-resistant, rendering it non-susceptible to all antibiotics across various antimicrobial categories [69]. *P. aeruginosa* ranks among the foremost pathogens responsible for healthcare-associated infections. The emergence of pandrug- resistance in problematic Gram-negative pathogens like *P. aeruginosa* among hospitalized patients presents a significant public health threat both globally and specifically in Egypt. Yearly reports highlight increasing rates of drug-resistant bacteria [70], and in Egypt, escalating rates of resistance have been documented and linked to the indiscriminate use of antibiotics in hospital settings [4, 5].

In-vitro antimicrobial activity of Col-Ag NPs, and Col-Ag-CuO NPs

Our findings indicate that both preparations exhibited clear zones of inhibition with minimal influence of concentration on the zone diameter. However, the zones produced by the Col-Ag-CuO NPs were generally larger, as depicted in Fig. 6.

A significant reduction in the MIC of colistin was observed in both preparations compared to colistin alone. The MIC values were 8 µg/mL for colistin alone, 0.046 µg/mL for Col-Ag NPs, and 0.0117 µg/mL for Col-Ag-CuO NPs. Additionally, there was a fourfold reduction in the MIC of bimetallic Col-Ag-CuO NPs compared to Col-Ag NPs, as shown in Fig. 6. Previous studies have reported higher activity of Ag NPs against *P. aeruginosa* when conjugated with colistin compared to Ag NPs alone [1, 71]. Similarly, antibacterial activity of CuO NPs has been documented [72]. However, to our knowledge, there have been no previous reports on bimetallic Ag-CuO
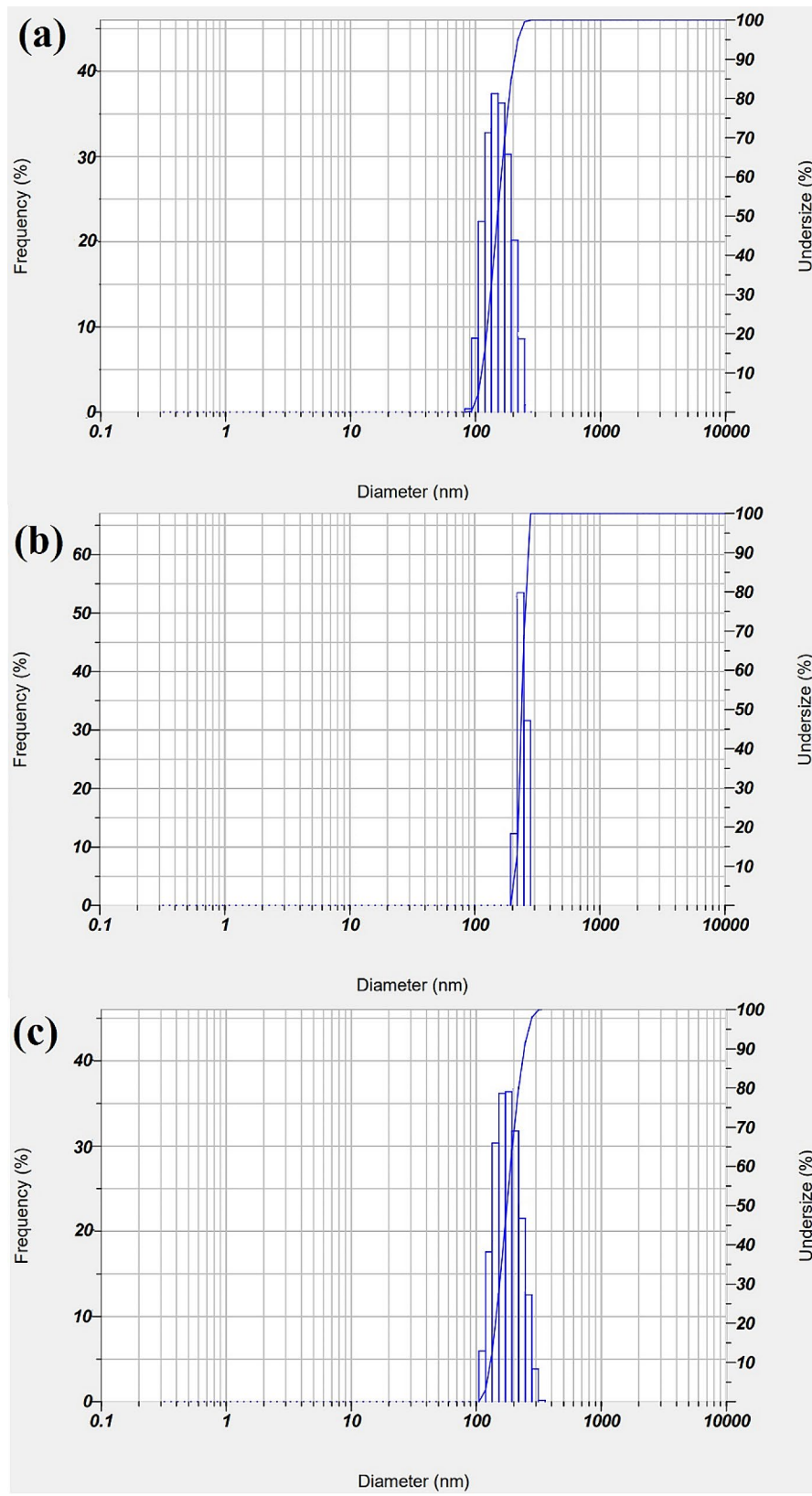
Fig. 4 DLS distribution analysis of the synthesized **(a)** Col-Ag NPs, **(b)** Col-CuO NPs, and **(c)** bimetallic Col-Ag-CuO NPs
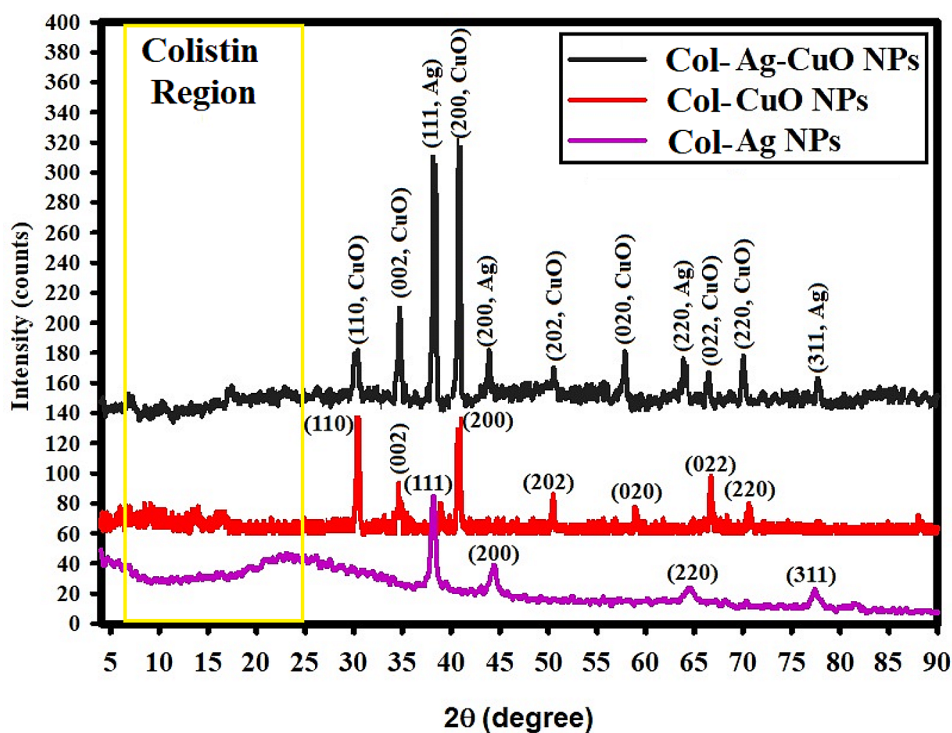
Fig. 5 XRD analysis of the synthesized Col-Ag NPs, Col-CuO NPs, and bimetallic Col-Ag-CuO NPs

NPs alloy nanoparticles conjugated with colistin to assess their antibacterial activity against the gram-negative pathogen *P. aeruginosa*. Consequently, our results highlight the effective antibacterial activity of Col-Ag-CuO NPs. These findings underscore the importance of bimetallic nanoparticles conjugated with colistin as potential alternatives for treating problematic superbugs in critically ill hospitalized patients.

Assessment of anti-virulent activity of Col-Ag-CuO NPs nanocomposite

Motility

As shown in Fig. 7, both swarming and twitching motility were noticeably reduced with increasing nanocomposite concentration compared to the control (absence of the nanocomposite). Specifically, a reduction of 32% and 64% in the swarm zone was observed with concentration 1 (0.29×10^{-2} µg/mL) and concentration 2 (0.58×10^{-2} µg/mL), respectively. Similarly, twitching motility was reduced by 34% and 97%, respectively. Using ANOVA, a statistically significant difference was found on increasing nanocomposite concentration compared to the control. The P values were $P < 0.0001$ for swarming motility and $P = 0.0005$ for twitching motility.

The pathogenicity of *P. aeruginosa* and its capacity to establish infections and cause diseases are primarily attributed to the array of virulence factors it secretes [47, 73]. These secreted virulence factors play crucial roles in modulating the immune response and facilitating bacterial colonization [73]. In our study, we observed that the synthesized nanoparticles not only displayed antimicrobial properties against *P. aeruginosa* but also hindered its mobility.

This observation holds significance as mobility is often linked to the virulence of bacterial pathogens, including *P. aeruginosa*. Virulence factors empower bacteria to colonize and infiltrate host tissues, evade host immune responses, and induce disease. The mobility inhibition by the nanoparticles implies a potential interference with the expression or function of virulence factors associated with bacterial motility.

Moreover, the antimicrobial effect of the nanoparticles suggests their capability to directly impede bacterial growth and viability, thereby potentially influencing the expression of virulence factors. Although our study did not delve into the specific mechanisms underlying the interplay between nanoparticle activity, mobility inhibition, and virulence factor expression, it offers valuable preliminary insights into the potential multifaceted effects of the synthesized nanoparticles on *P. aeruginosa*.

Therefore, the activity of the bimetallic colistin nanoconjugation (Col-Ag-CuO NPs) against the secreted virulence factors of *P. aeruginosa* presents promising treatment options. This is particularly crucial given the formidable challenge posed by *P. aeruginosa* exceptional ability to acquire resistance to various antibiotics and undergo rapid mutations.
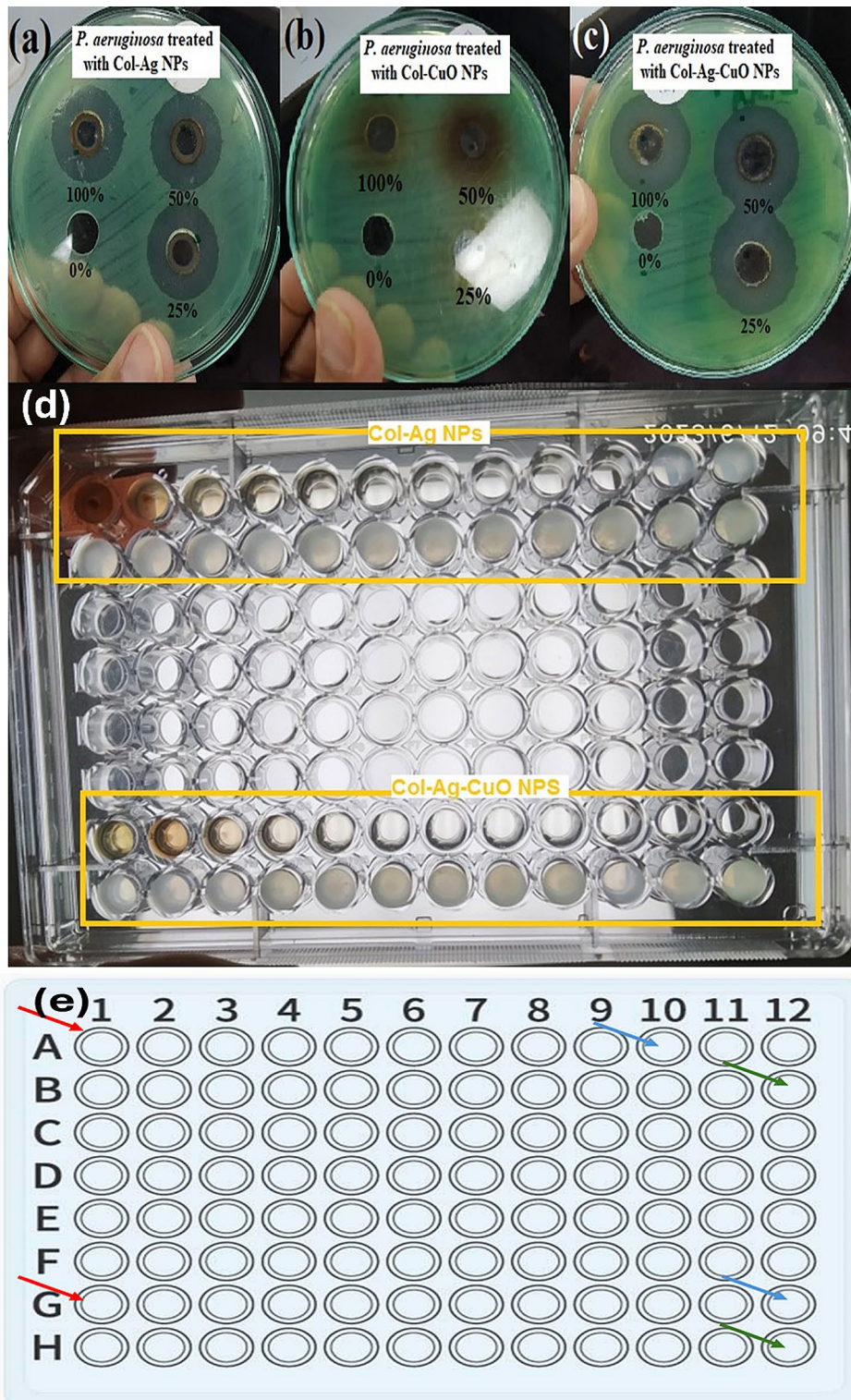
Fig. 6 **(a, b** and **c)**. Agar well diffusion assay was performed to evaluate the antimicrobial activity of the three nanocomposite solutions at varying concentrations. **(d)**. Minimum Inhibitory Concentration (MIC) using broth microdilution method. **(e)**. Illustration panel for the MIC; rows A&B representing the dilution range of Col-Ag NPs, while **G** &**H** representing the dilution range of Col-Ag-CuO NPS, red arrows pointing to the highest concentration of the alloy (25 µg/ml), green arrows pointing to the lowest concentration of the alloys (3×10^{-6} µg/ml), blue arrows pointing to the MIC
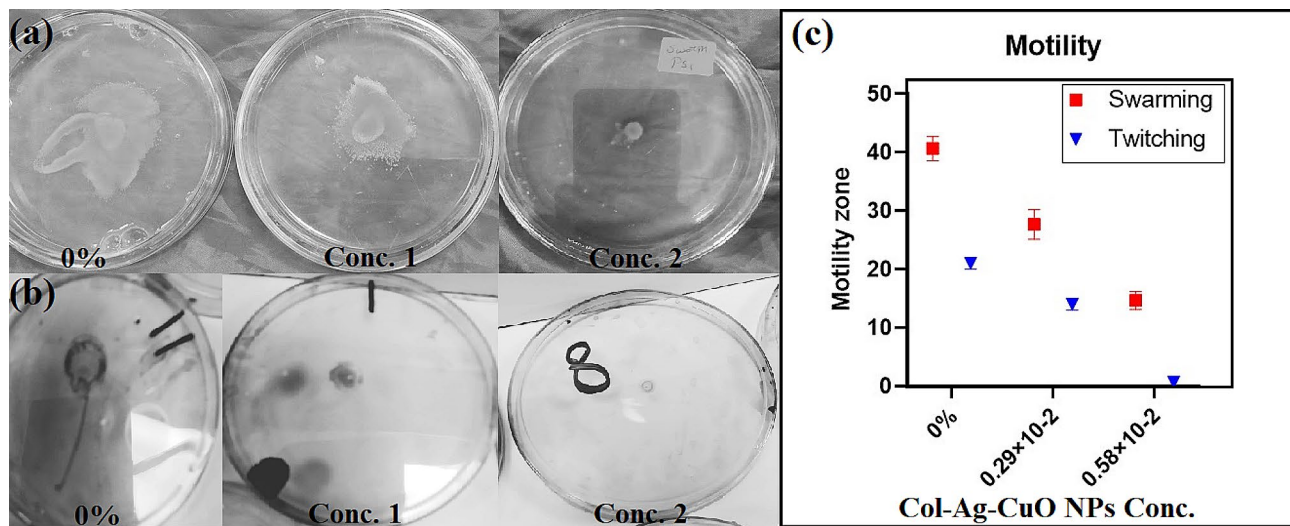
Fig. 7 The effect of bimetallic Col-Ag-CuONPs on *P. aeruginosa* motility **(a)** reduction in swarm zone **(b)** reduction in twitching motility **(c)** The average of the 3 different readings with regard to each concentration
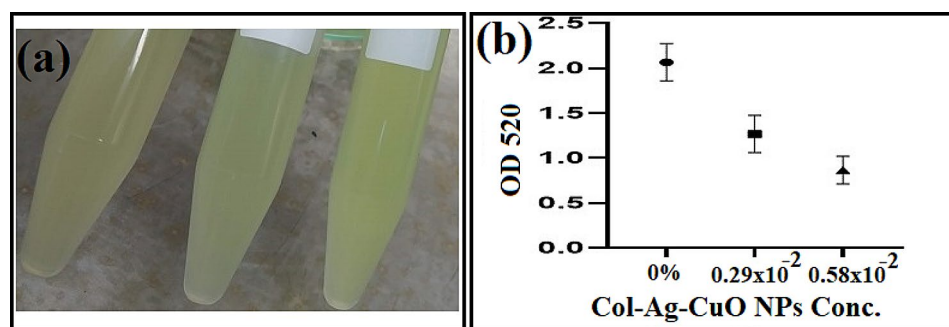

Fig. 8 The effect of bimetallic Col-Ag-CuONPs on Pyocyanin production of *P. aeruginosa*. **(a)** Reduction in pigment production. **(b)** Means of 3 OD_{520} readings

Pyocyanin production

One of the significant virulence factors of *P. aeruginosa*, contributing to its pathogenicity and severity of infections, is the production of the blue-green pigment pyocyanin [74]. Pyocyanin is known to induce tissue injury by generating reactive oxygen species [75]. The OD_{520} values of extracted pyocyanin were notably decreased following *P. aeruginosa* exposure to concentration 1 (0.29×10^{-2} µg/mL) and concentration 2 (0.58×10^{-2} µg/mL) of the bimetallic Col-Ag-CuO NPs nanocomposite. A reduction of 39% and 58% was observed compared to the OD_{520} value of pyocyanin extracted from the non-treated sample (Fig. 8). A statistically significant difference was observed on increasing nanocomposite concentration compared to the control. The P values was 0.0015.

Biofilm formation

The two sub-inhibitory concentrations of the nanocomposite exhibited concentration-dependent antibiofilm activity against our strong biofilm-producing *P. aeruginosa* isolate. Biofilm inhibition percentages were compared to the control sample at 570 nm wavelength. The higher concentration (conc 2 = 0.58×10^{-2} µg/mL) demonstrated the most effective biofilm inhibition at 48%, while the lower concentration (conc 1 = 0.29×10^{-2} µg/mL) reduced biofilm formation by 33%. A statistically significant difference was noticed between different treatments ($P < 0.0001$). Supportive evidence was obtained through viable counts of biofilm cells in the absence and presence of the nanocomposite. Higher concentrations decreased the viability of sessile cells by approximately 1.2 log CFU compared to the control (Fig. 9a and b). Combining results from plate-based assays and bacterial cell count assays, it can be concluded that the nanocomposite inhibited *P. aeruginosa* biofilm formation.

Eradication of mature biofilm was also observed when challenged with the bimetallic Col-Ag-CuO NPs nanocomposite compared to the control. This eradication occurred in a concentration-dependent manner: 30% and 17.7% for the higher and lower concentrations, respectively. A statistically significant difference was noticed between different treatments ($P = 0.0037$).
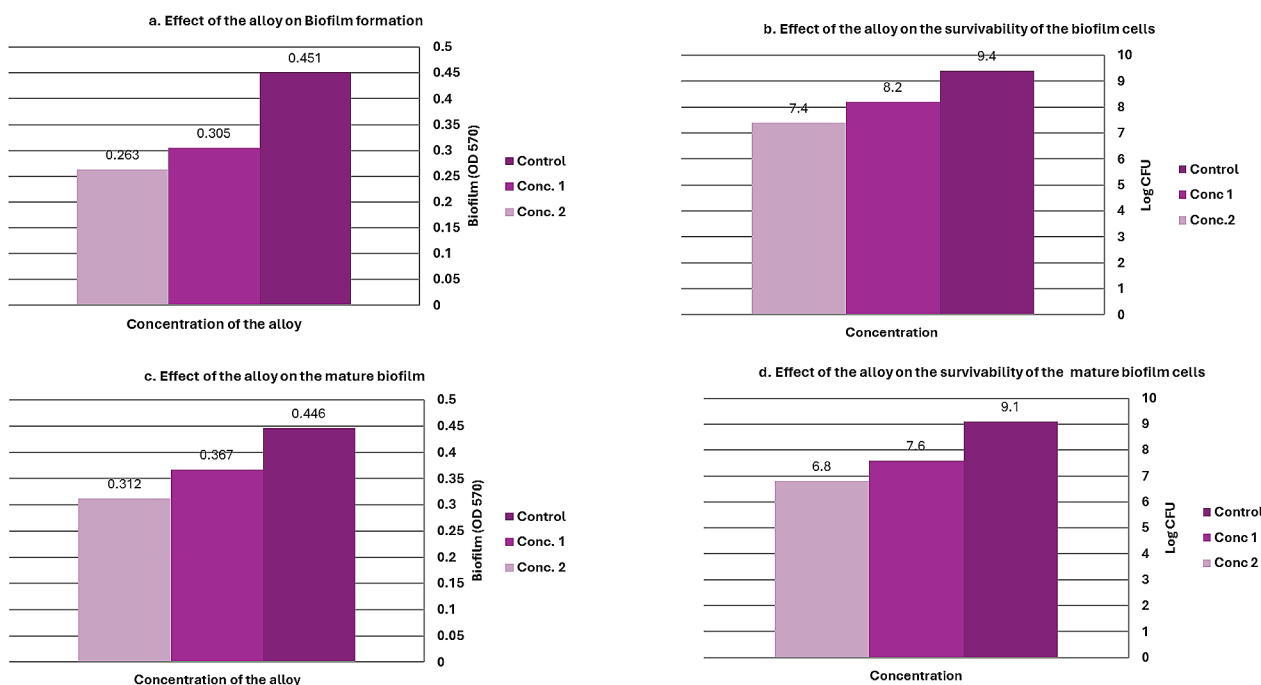
Fig. 9 The effect of bimetallic Col-Ag-CuONPs on biofilm formation of *P. aeruginosa*

This is further supported by colony counts of biofilm cells, which were reduced by approximately 2.3 log CFU and 1.5 log CFU (Fig. 9c and d).

One of the main challenges in treating *P. aeruginosa* infections is the complex structure of its biofilm, which enables it to evade the immune system, making infections difficult to treat [76]. Various studies have assessed the activity of Ag NPs in hindering the biofilm formation ability of gram-negative pathogens such as *A. baumannii*, *P. aeruginosa* (synergy with tobramycin), *E. coli*, and *K. pneumoniae* [77–80]. However, this study represents the first report of decreasing biofilm activity in a strong biofilm producer *P. aeruginosa* clinical isolate using Col-Ag-CuO nano-preparation.

In vivo activity of Col-Ag-CuO NPs nanocomposite using *G. mellonella* model

Few studies have described the toxicity of NP-antimicrobials with controversies. However, despite several studies, the current available information is insufficient to ascertain the adverse effects of NP-antimicrobials on human health. Therefore, it is imperative that further research be carried out to determine the safety profile of NP-antimicrobials to mitigate any toxicological problems that may arise.

In this study, the cytotoxic effect of the Ag-CuO NPs-based colistin combination against *G. mellonella* model was evaluated to gain some insight into the safety of the tested combination. The results indicate that the nanocomposite is non-toxic for *G. mellonella*, showing similar

survival rates as the saline-treated group (100% survival by day 3). Additionally, there was observed attenuation of the virulence of the *P. aeruginosa* isolate challenged with the nanocomposite compared to the control group. This attenuation occurred in a concentration-dependent manner, as demonstrated in the survival curve (Fig. 10).

The *Galleria mellonella* in vivo model offers technical, cost and ethical advantages for evaluating novel antimicrobial agents relative to mammalian models [81]. The combination of high virulence and pan-drug resistance in the isolate against commonly used antimicrobials could significantly impact morbidity and mortality rates associated with *P. aeruginosa* infections.

The findings of this study reveal that the isolate recovered from the blood of a pediatric hospitalized cancer patient is highly virulent and pan-drug resistant, posing a significant threat to patients and hospital settings while complicating therapeutic options. The data presented will require further studies before effective 'treatment options' can be developed.

Pseudomonas aeruginosa protein leakage investigation

The amount of *P. aeruginosa* protein removed (assumably as a result of pore formation which helped in making the proteins bleed out from the P. aeruginosa cytoplasm) is directly proportional to the concentration of Col-Ag NPs, and bimetallic Col-Ag-CuO NPs; it was estimated to be 207.44 μg/mL, and 404.23 μg/mL following the treatment with Col-Ag NPs and bimetallic Col-Ag-CuO NPs, respectively (1.0 mg/mL) (Fig. 11). As damage caused by
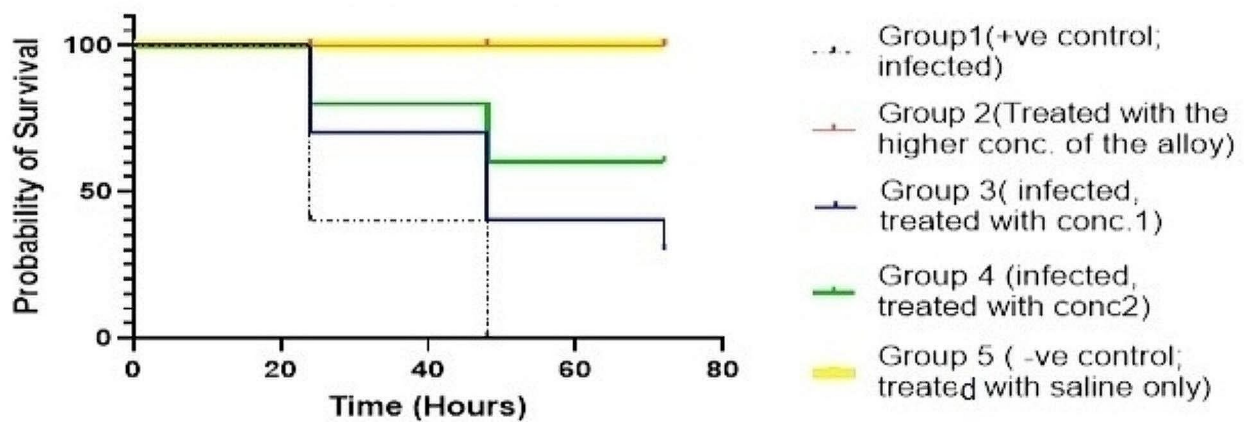
Fig. 10 Kaplan Meier survival curve showing the effect of bimetallic Col-Ag-CuO NPs on survival of *G. melonella* infected with *P. aeruginosa*, where Group 1 is positive control; infected, Group 2 is treated with high concentration of Col-Ag-CuO NPs, Group 3 is infected and treated with concentration 1, Group 4 is infected and treated with concentration 2, Group 5 is negative control; treated with saline only
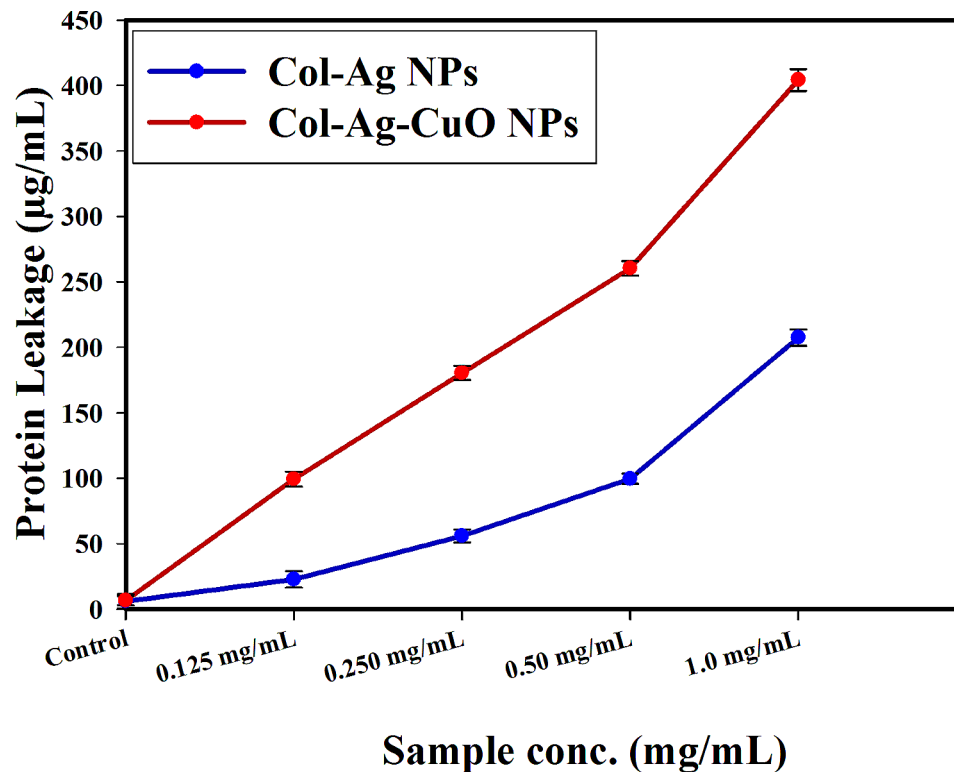

Fig. 11 The effect of Col-Ag NPs, and bimetallic Col-Ag-CuO NPs on the protein leakage from *P. aeruginosa* cell membranes

the NPs progresses overtime, the leakage of cellular constituents induces cell collapse, further scoring the importance of this assay in determining cell integrity.

Similar results were reported in recent publications [82, 83]; combined NPs showed concentration-dependence for the dislodgement in the bacterial membrane and suggested leakage of bacterial intracellular organelles into the extracellular cell structure.

Ag NPs have a multi-level mode of action influencing many bacterial structures and metabolic processes including inactivating bacterial enzymes [84], disrupting cell wall, metabolic processes [85], and increasing cell permeability [86, 87]. Ag NPs can also interact with DNA [84], or generate reactive oxygen species [88], which damage biomacromolecules [89].

Nanomolecules (NM) act along two major lethal pathways, which are related to each other and in many cases

occur simultaneously. The antimicrobial properties of Ag NPs can be attributed to multiple different mechanisms, including: (i) disruption of cell membrane integrity resulting in pore formation in treated bacterial cells leading to an increase in permeability allowing antibiotics to enter the cells more easily, and (ii) production of reactive oxygen-free radicals with the NM acting as nano-catalysts.

Figure 11 shows the effect of Col-Ag NPs and bimetallic Col-Ag-CuO NPs on the protein leakage from *P. aeruginosa* cell membrane. Protein leakage assay and/or SEM imaging are used for evaluating the antimicrobial potential of synthesized nanoparticles [39]. In some studies, SEM imaging process was used to confirm the pore formation in the treated bacterial cells [39, 90, 91]. In this study, the protein leakage assay was used to assess *P. aeruginosa* integrity following treatment with NPs in comparison with non-treated control.

Conclusion

This study investigated the use of bimetallic silver-copper oxide nanoparticles (Ag-CuO NPs) conjugated with colistin to combat a highly virulent, pandrug-resistant clinical isolate of *P. aeruginosa.* The combination significantly lowered the minimum inhibitory concentration (MIC) of colistin and decreased swarming and twitching motility, pyocyanin production, and biofilm formation of *P. aeruginosa.* Additionally, the nanoparticles were non-toxic to *Galleria mellonella*, showing 100% survival, comparable to saline-treated controls. This research offers a promising approach to tackle antibiotic-resistant *P. aeruginosa* strains, including those resistant to colistin. By leveraging the synergistic effects of silver and copper oxide nanoparticles, the study presents a novel method to combat resistant infections through mechanisms such as reactive oxygen species generation and membrane disruption. The positive results suggest that colistin-conjugated Ag-CuO NPs could be developed for treating difficult infections, particularly in immunocompromised patients. Furthermore, the findings could inform nanoparticle-based therapies against other multidrug-resistant pathogens, aiding global efforts to combat antimicrobial resistance. However further research is needed to consolidate the reported findings.

Author details
[1]Department of Microbiology and Immunology, Faculty of Pharmacy, Ahram Canadian University, Giza, Egypt
[2]Department of Microbiology and Immunology, Faculty of Pharmacy, Cairo University, Cairo, Egypt
[3]Department of Clinical Pathology, National Cancer Institute, Cairo University, Cairo, Egypt
[4]Department of Microbiology and Immunology, Faculty of Pharmacy, Galala University, New Galala City, Suez, Egypt
[5]Drug Microbiology Lab, Drug Radiation Research Department, National Center for Radiation Research and Technology (NCRRT), Egyptian Atomic Energy Authority (EAEA), Cairo, Egypt

References
1. Thomaz L et al. In vivo activity of silver nanoparticles against Pseudomonas aeruginosa infection in Galleria mellonella. Front Microbiol, 2020: p. 2798.
2. Organization WH. *WHO publishes list of bacteria for which new antibiotics are urgently needed. February 27, 2017.* 2023.
3. Paprocka P, et al. Pseudomonas aeruginosa infections in cancer patients. Pathogens. 2022;11(6):679.
4. El-Mahallawy HA, et al. Increasing trends of colistin resistance in patients at high-risk of carbapenem-resistant Enterobacteriaceae. Ann Med. 2022;54(1):2748–56.
5. Zafer MM et al. *Antimicrobial resistance pattern and their beta-lactamase encoding genes among Pseudomonas aeruginosa strains isolated from cancer patients* BioMed research international, 2014. 2014.
6. Shabban M, et al. Resistance to colistin mediated by mcr-1 among multidrug resistant Gram negative pathogens at a tertiary care hospital, Egypt. J Pure Appl Microbiol. 2020;14(2):1125–32.
7. Karaiskos I, Antoniadou A, Giamarellou H. Combination therapy for extensively-drug resistant gram-negative bacteria. Expert Rev anti-infective Therapy. 2017;15(12):1123–40.
8. Shrivastava SR, Shrivastava PS, Ramasamy J. World health organization releases global priority list of antibiotic-resistant bacteria to guide research, discovery, and development of new antibiotics. J Med Soc. 2018;32(1):76–7.

9.   Aslam B et al. *Antibiotic resistance: a rundown of a global crisis* Infection and drug resistance, 2018: pp. 1645–1658.

10. Dadgostar P. *Antimicrobial resistance: implications and costs* Infection and drug resistance, 2019: pp. 3903–3910.

11. Perez F, Adachi J, Bonomo RA. Antibiotic-resistant gram-negative bacterial infections in patients with cancer. Clin Infect Dis. 2014;59(suppl5):S335–9.

12. Alabresm A, et al. Nanotargeting of resistant infections with a special emphasis on the biofilm landscape. Bioconjug Chem. 2021;32(8):1411–30.

13. El-Behery RR, El-Sayed E-SR, El-Sayyad GS. Gamma rays-assisted bacterial synthesis of bimetallic silver-selenium nanoparticles: powerful antimicrobial, antibiofilm, antioxidant, and photocatalytic activities. BMC Microbiol. 2023;23(1):1–18.

14. Lakshmi S, et al. Hybrid of Metapenaeus dobsoni lectin and platinum nanoparticles exert antimicrobial and immunostimulatory effects to reduce bacterial bioburden in infected Nile tilapia. Sci Rep. 2023;13(1):525.

15. Khalil MA, El GM, Maghraby. Enhanced efficacy of some antibiotics in presence of silver nanoparticles against multidrug resistant Pseudomonas aeruginosa recovered from burn wound infections. Front Microbiol. 2021;12:648560.

16. Paladini F, Pollini M. Antimicrobial silver nanoparticles for wound healing application: progress and future trends. Materials. 2019;12(16):2540.

17. Li X et al. *Biosynthesis of nanoparticles by microorganisms and their applications* Journal of Nanomaterials, 2011. 2011.

18. Godipurge S, et al. A facile and green strategy for the synthesis of au, ag and Au–Ag alloy nanoparticles using aerial parts of R. Hypocrateriformis extract and their biological evaluation. Enzym Microb Technol. 2016;95:174–84.

19. Hashem AH, El-Sayyad GS. Antimicrobial and anticancer activities of biosynthesized bimetallic silver-zinc oxide nanoparticles (Ag-ZnO NPs) using pomegranate peel extract. Biomass Convers Biorefinery, 2023: p. 1–13.

20. Liu R, et al. Alloyed crystalline Au–Ag hollow nanostructures with high chemical stability and catalytic performance. ACS Appl Mater Interfaces. 2016;8(26):16833–44.

21. El-Batal AI, Mosallam FM, El-Sayyad GS. *Synthesis of Metallic Silver Nanoparticles by Fluconazole Drug and Gamma Rays to Inhibit the Growth of Multidrug-Resistant Microbes* Journal of Cluster Science: pp. 1–13.

22. Bryaskova R, et al. Synthesis and comparative study on the antimicrobial activity of hybrid materials based on silver nanoparticles (AgNps) stabilized by polyvinylpyrrolidone (PVP). J Chem Biol. 2011;4(4):185.

23. CLSI M. Performance standards for antimicrobial susceptibility testing. Wayne, PA USA: CLSI; 2019.

24. *European Committee on Antimicrobial Susceptibility Testing, Breakpoint tables for interpretation of MICs and zone diameters*. 2015, European Society of Clinical Microbiology and Infectious Diseases Basel &#8230.

25. Balouiri M, Sadiki M, Ibnsouda SK. Methods for in vitro evaluating antimicrobial activity: a review. J Pharm Anal. 2016;6(2):71–9.

26. Kowalska-Krochmal B, Dudek-Wicher R. The minimum inhibitory concentration of antibiotics: methods, interpretation, clinical relevance. Pathogens. 2021;10(2):165.

27. Wang S, et al. Inhibition of virulence factors and biofilm formation by wogonin attenuates pathogenicity of Pseudomonas aeruginosa PAO1 via targeting pqs quorum-sensing system. Int J Mol Sci. 2021;22(23):12699.

28. Lee JH, Cho MH, Lee J. 3-Indolylacetonitrile decreases Escherichia coli O157: H7 biofilm formation and Pseudomonas aeruginosa virulence. Environ Microbiol. 2011;13(1):62–73.

29. Elbasuney S, et al. Antimicrobial, and antibiofilm activities of silver doped hydroxyapatite: a novel bioceramic material for dental filling. J Inorg Organomet Polym Mater. 2022;32(12):4559–75.

30. Pham DTN, et al. Biofilm inhibition, modulation of virulence and motility properties by FeOOH nanoparticle in Pseudomonas aeruginosa. Brazilian J Microbiol. 2019;50:791–805.

31. Thomaz L, et al. In vivo activity of silver nanoparticles against Pseudomonas aeruginosa infection in Galleria mellonella. Front Microbiol. 2020;11:582107.

32. Agarwal H, et al. Eco-friendly synthesis of zinc oxide nanoparticles using Cinnamomum Tamala leaf extract and its promising effect towards the antibacterial activity. J Drug Deliv Sci Technol. 2019;53:101212.

33. Brownlee K. Probit Analysis: a statistical treatment of the Sigmoid response curve. JSTOR; 1952.

34. El-Sayyad GS, Mosallam FM, El-Batal AI. One-pot green synthesis of magnesium oxide nanoparticles using Penicillium chrysogenum melanin pigment and gamma rays with antimicrobial activity against multidrug-resistant microbes. Adv Powder Technol. 2018;29(11):2616–25.

35. El-Batal AI, et al. Factorial design-optimized and gamma irradiation-assisted fabrication of selenium nanoparticles by chitosan and pleurotus ostreatus fermented fenugreek for a vigorous in vitro effect against carcinoma cells. Int J Biol Macromol. 2020;156:1584–99.

36. Składanowski M, et al. Silver and gold nanoparticles synthesized from Streptomyces sp. isolated from acid forest soil with special reference to its antibacterial activity against pathogens. J Cluster Sci. 2017;28(1):59–79.

37. Link S, El-Sayed MA. Optical properties and ultrafast dynamics of metallic nanocrystals. Annu Rev Phys Chem. 2003;54(1):331–66.

38. El-Batal AI, et al. Gum arabic polymer-stabilized and Gamma rays-assisted synthesis of bimetallic silver-gold nanoparticles: powerful antimicrobial and antibiofilm activities against pathogenic microbes isolated from diabetic foot patients. Int J Biol Macromol. 2020;165:169–86.

39. Elakraa AA, et al. Cefotaxime incorporated bimetallic silver-selenium nanoparticles: promising antimicrobial synergism, antibiofilm activity, and bacterial membrane leakage reaction mechanism. RSC Adv. 2022;12(41):26603–19.

40. Hashem AH, El-Sayyad GS. Antimicrobial and anticancer activities of biosynthesized bimetallic silver-zinc oxide nanoparticles (Ag-ZnO NPs) using pomegranate peel extract. Biomass Conversion and Biorefinery; 2023.

41. Gaber SE, et al. Antifungal activity of myco-synthesized bimetallic ZnO-CuO nanoparticles against fungal plant pathogen Fusarium oxysporum. Biomass Conversion and Biorefinery; 2023.

42. El-Behery RR, El-Sayed E-SR, El-Sayyad GS. Gamma rays-assisted bacterial synthesis of bimetallic silver-selenium nanoparticles: powerful antimicrobial, antibiofilm, antioxidant, and photocatalytic activities. BMC Microbiol. 2023;23(1):224.

43. El-Batal AI, et al. Gum arabic-assisted biomass synthesis of bimetallic ZnO-CuO nanoparticles using gamma rays for controlling potato post-harvest tuber rots-causing Alternaria solani: towards improving food safety. Biomass Conversion and Biorefinery; 2023.

44. Attia MS, et al. Protective role of Mycosynthesized Bimetallic ZnO-CuO nanoparticles as therapeutic nutrients to enhance the resistance of Vicia faba against Fusarium Wilt Disease. Agronomy. 2023;13(11):2725.

45. Elkhodary BH, et al. Effectiveness of bimetallic ZnO-B2O3 nanoparticles produced by Streptomyces gancidicus as prospective antifungal agents and therapeutic nutrients to enhance pea plant immunity against damping off-causing Pythium irregulare: in vivo and in vitro investigations. Biomass Conversion and Biorefinery; 2023.

46. Hashem AH, et al. Watermelon rind mediated biosynthesis of bimetallic selenium-silver nanoparticles: characterization, Antimicrobial and Anticancer activities. Plants. 2023;12(18):3288.

47. Mostafa HY, et al. Promising antimicrobial and antibiofilm activities of Orobanche Aegyptiaca extract-mediated bimetallic silver-selenium nanoparticles synthesis: Effect of UV-exposure, bacterial membrane leakage reaction mechanism, and kinetic study. Arch Biochem Biophys. 2023;736:109539.

48. El-Batal AI, et al. Gum arabic assisted the biomass synthesis of bimetallic silver copper oxide nanoparticles using gamma-rays for improving bacterial and viral wound healing: promising antimicrobial activity against foot and mouth disease. Int J Biol Macromol. 2024;262:130010.

49. El-Batal AI, et al. Antimicrobial synergism and antibiofilm activity of Amoxicillin loaded citric acid-magnesium ferrite nanocomposite: Effect of UV-illumination, and membrane leakage reaction mechanism. Microb Pathog. 2022;164:105440.

50. Mohsin M, et al. An insight into the Coating Behavior of Bimetallic Silver and Gold Core-Shell Nanoparticles. PLASMONICS; 2020.

51. Gopinath K, et al. Green synthesis of silver, gold and silver/gold bimetallic nanoparticles using the Gloriosa superba leaf extract and their antibacterial and antibiofilm activities. Microb Pathog. 2016;101:1–11.

52. Loza K, Heggen M, Epple M. Synthesis, structure, Properties, and applications of bimetallic nanoparticles of Noble metals. Adv Funct Mater. 2020;30(21):1909260.

53. Borah R, Verbruggen SW. Silver-gold Bimetallic Alloy versus Core-Shell nanoparticles: implications for Plasmonic Enhancement and Photothermal Applications. The Journal of Physical Chemistry C; 2020.

54. Clément M, et al. Gold (I)–silver (I)–calix [8] arene complexes, precursors of bimetallic alloyed Au–Ag nanoparticles. Nanoscale Advances; 2020.

55. Castro-Longoria E, Vilchis-Nestor AR, Avalos-Borja M. Biosynthesis of silver, gold and bimetallic nanoparticles using the filamentous fungus Neurospora Crassa. Colloids Surf B. 2011;83(1):42–8.

56. Han SW, Kim Y, Kim K. Dodecanethiol-derivatized Au/Ag bimetallic nanoparticles: TEM, UV/VIS, XPS, and FTIR analysis. J Colloid Interface Sci. 1998;208(1):272–8.

57. Govindaraju K, et al. Silver, gold and bimetallic nanoparticles production using single-cell protein (Spirulina platensis) Geitler. J Mater Sci. 2008;43(15):5115–22.

58. Garcia PR, et al. An in situ SAXS investigation of the formation of silver nanoparticles and bimetallic silver–gold nanoparticles in controlled wet-chemical reduction synthesis. Nanoscale Adv. 2020;2(1):225–38.

59. Zou X, Ying E, Dong S. Preparation of novel silver–gold bimetallic nanostructures by seeding with silver nanoplates and application in surface-enhanced Raman scattering. J Colloid Interface Sci. 2007;306(2):307–15.

60. El-Batal AI, et al. Biogenic synthesis of copper nanoparticles by natural polysaccharides and Pleurotus Ostreatus fermented fenugreek using gamma rays with antioxidant and antimicrobial potential towards some wound pathogens. Microb Pathog. 2018;118:159–69.

61. Baraka A, et al. Synthesis of silver nanoparticles using natural pigments extracted from Alfalfa leaves and its use for antimicrobial activity. Chem Pap. 2017;71(11):2271–81.

62. Awed AS, et al. Unveiling antimicrobial activity of Metal Iodide (CuI, AgI, and PbI2) nanoparticles: towards Biomedical surfaces Applications. Journal of Cluster Science; 2019.

63. Jyoti K, Baunthiyal M, Singh A. Characterization of silver nanoparticles synthesized using Urtica dioica Linn. Leaves and their synergistic effects with antibiotics. J Radiation Res Appl Sci. 2016;9(3):217–27.

64. Siddiquee MA, et al. Biogenic synthesis, in-vitro cytotoxicity, esterase activity and interaction studies of copper oxide nanoparticles with lysozyme. J Mater Res Technol. 2021;13:2066–77.

65. Bigdeli F, Morsali A. Synthesis ZnO nanoparticles from a new zinc (II) coordination polymer precursor. Mater Lett. 2010;64(1):4–5.

66. Poyraz S, et al. One-step synthesis and characterization of polyaniline nanofiber/silver nanoparticle composite networks as antibacterial agents. ACS Appl Mater Interfaces. 2014;6(22):20025–34.

67. Belavi P, et al. Structural, electrical and magnetic properties of cadmium substituted nickel–copper ferrites. Mater Chem Phys. 2012;132(1):138–44.

68. Pal K, Elkodous MA, Mohan MM. CdS nanowires encapsulated liquid crystal in-plane switching of LCD device. J Mater Sci: Mater Electron. 2018;29(12):10301–10.

69. Magiorakos A-P, et al. Multidrug-resistant, extensively drug-resistant and pandrug-resistant bacteria: an international expert proposal for interim standard definitions for acquired resistance. Clin Microbiol Infect. 2012;18(3):268–81.

70. Litwin A, Fedorowicz O, Duszynska W. Characteristics of microbial factors of healthcare-associated infections including multidrug-resistant pathogens and antibiotic consumption at the university intensive care unit in Poland in the years 2011–2018. Int J Environ Res Public Health. 2020;17(19):6943.

71. Wali N, et al. Synergistic efficacy of colistin and silver nanoparticles impregnated human amniotic membrane in a burn wound infected rat model. Sci Rep. 2022;12(1):6414.

72. Singh D, et al. Bacteria assisted green synthesis of copper oxide nanoparticles and their potential applications as antimicrobial agents and plant growth stimulants. Front Chem. 2023;11:1154128.

73. Qin S, et al. Pseudomonas aeruginosa: Pathogenesis, virulence factors, antibiotic resistance, interaction with host, technology advances and emerging therapeutics. Signal Transduct Target Therapy. 2022;7(1):199.

74. Edward EA, et al. Prevalence of different virulence factors and their association with antimicrobial resistance among Pseudomonas aeruginosa clinical isolates from Egypt. BMC Microbiol. 2023;23(1):1–13.

75. Muller M. Pyocyanin induces oxidative stress in human endothelial cells and modulates the glutathione redox cycle. Free Radic Biol Med. 2002;33(11):1527–33.

76. Tuon FF, et al. Pathogenesis of the Pseudomonas aeruginosa biofilm: a review. Pathogens. 2022;11(3):300.

77. Singh R, et al. Antibacterial activities of bacteriagenic silver nanoparticles against nosocomial Acinetobacter baumannii. J Nanosci Nanotechnol. 2018;18(6):3806–15.

78. Habash MB, et al. Potentiation of tobramycin by silver nanoparticles against Pseudomonas aeruginosa biofilms. Antimicrob Agents Chemother. 2017;61(11). https://doi.org/10.1128/aac. 00415–17.

79. Shafreen RB, et al. Inhibitory effect of biosynthesized silver nanoparticles from extract of Nitzschia palea against curli-mediated biofilm of Escherichia coli. Appl Biochem Biotechnol. 2017;183:1351–61.

80. Farooq U et al. Rifampicin conjugated silver nanoparticles: a new arena for development of antibiofilm potential against methicillin resistant Staphylococcus aureus and Klebsiella pneumoniae. Int J Nanomed, 2019: p. 3983–93.

81. Beeton M, et al. Assessing phage therapy against Pseudomonas aeruginosa using a Galleria mellonella infection model. Int J Antimicrob Agents. 2015;46(2):196–200.

82. Rajesh S, Dharanishanthi V, Kanna AV. Antibacterial mechanism of biogenic silver nanoparticles of Lactobacillus acidophilus. J Exp Nanosci. 2015;10(15):1143–52.

83. Azam Z, et al. Microbial synthesized cadmium oxide nanoparticles induce oxidative stress and protein leakage in bacterial cells. Microb Pathog. 2020;144:104188.

84. Li W-R, et al. Antibacterial effect of silver nanoparticles on Staphylococcus aureus. Biometals. 2011;24:135–41.

85. Cui L, et al. In situ study of the antibacterial activity and mechanism of action of silver nanoparticles by surface-enhanced Raman spectroscopy. Anal Chem. 2013;85(11):5436–43.

86. Morones JR, et al. The bactericidal effect of silver nanoparticles. Nanotechnology. 2005;16(10):2346.

87. Saravanan M, et al. Synthesis of silver nanoparticles from Phenerochaete chrysosporium (MTCC-787) and their antibacterial activity against human pathogenic bacteria. Microb Pathog. 2018;117:68–72.

88. Xu H, et al. Role of reactive oxygen species in the antibacterial mechanism of silver nanoparticles on Escherichia coli O157: H7. Biometals. 2012;25:45–53.

89. Cabiscol Catalã E, Sumalla JT, Ros J, Salvador. Oxidative Stress bacteria Protein Damage Reactive Oxygen Species 2000.

90. El-Sayyad GS, et al. Gentamicin-assisted mycogenic selenium nanoparticles synthesized under Gamma Irradiation for Robust Reluctance of resistant urinary tract infection-causing pathogens. Biol Trace Elem Res. 2020;195(1):323–42.

91. El-Batal AI, et al. Nystatin-mediated bismuth oxide nano-drug synthesis using gamma rays for increasing the antimicrobial and antibiofilm activities against some pathogenic bacteria and Candida species. RSC Adv. 2020;10(16):9274–89.

Publisher's Note